IIETA International Information and Engineering Technology Association
Advancing the World of Information and Engineering

Mathematical Modelling of Engineering Problems
Vol. 12, No. 4, April, 2025, pp. 1343-1352
Journal homepage: http://iieta.org/journals/mmep

Design and Simulation of Adaptive Sliding Mode Fuzzy Controller for a 2-Link Robot Manipulator

Aya M. Hameed*, Ahmed Khalaf Hamoudi

Control and Systems Department, University of Technology-Iraq, Baghdad 10066, Iraq

Corresponding Author Email: cse.21.08@grad.uotechnology.edu.iq

https://doi.org/10.18280/mmep.120425

Received: 27 February 2024
Revised: 8 May 2024
Accepted: 15 May 2024
Available online: 30 April 2025

Keywords:
ASMC, CSMC, AFSMC, CSMFC, barrier function, saturation function, chatter

ABSTRACT

Sliding mode controllers (SMC) are among the most durable and nonlinear regulators. Its methodical design process gives a simple answer for the control signal. The main disadvantage is that a traditional SMC suffers from chatter, which creates an unwanted zigzag stir over the sliding face. numerous approaches were developed and applied to palliate the downsides of this traditional methodology. The purpose of this paper is to reduce the settling time and magnitude of chatter as small as possible by designing several regulators; a classical sliding mode controller (CSMC) with a saturation function (SF), a CSMC with a barrier function (BF), an adaptive sliding mode controller (ASMC) with a saturation function, a conventional sliding mode fuzzy controller (CSMFC) with a saturation function and an adaptive sliding mode fuzzy controller (ASMFC) with a saturation function. The issues of the simulations can be attained using MATLAB 2018a/Simulink. The modeling shows that the results of ASMFC and CSMFC are better than the results of ASMC with achromatism function, and CSMC with achromatism function and with barricade function because the magnitude of chatter in the control action has been important reduced to roughly zero value and they take small settling time in comparison with others.

1. INTRODUCTION

Robotics breakthroughs have had a substantial impact on the productivity and effectiveness of robotization activities. Robots are used in diligence to do various duties, like cutting, welding, putting together, selecting, and placing [1]. Nonlinear factors are the most important considerations. Unmodeled uncertainty in mechanical systems can also make system control delicate. likewise, the selector may have uncertainty or faults, with blights naturally regarded as a kind of query. The enterprises above, videlicet nonlinearity, query, and disturbances, hamper the regulator design system. Because not all control systems can give stability, robust control styles are needed to limit the impacts of uncertainty and disturbances [2]. SMC is deemed the absolute most trustworthy nonlinear controller. The systematic design creates a simple arrangement for the control signals. Since the SMC's lack of care for parameter query (pu) and external disturbances (ed) until the late 1970s, it got estimable consideration from the control interrogate about the community [3]. The SMC plan is divided into two central forms: recognizing a sliding surface (ss.) and providing a spastic control run the show, this causes the system's state way to arrive at the ss. at a particular moment and stay there from then on. Due to the nonlinear inflow and coupling associations, exact and vigorous control is worrisome. As a result, erecting a regulator using normal control strategies grounded on the inflow of the mechanical frame may be an errand, particularly when exercising the normal control setup [4]. As a result, it's critical to make a regulator with high performance, adaptability, stability, and a simpler approach for resolving the problem in the presence of external disturbances and parameter changes [5]. SMC is the most effective robust control technology for mollifying goods. It's an important fine fashion that yields a nonlinear robust regulator with respectable performance [6]. In fact, in SMC, the SF sat (s, φ) function can be used rather than the signum function sign (s) to drop the chatter. To reduce chatter, a BF function is used rather than the sign (s) or SF. The BF can guarantee that the affair variable converges to a near-zero value [7]. numerous approaches are proposed, and in this work, ASMFC, SMFC, ASMC, and in addition to CSMC are designed to tune the regulators' gain and exclude the chatter problem. These regulators can render the system asymptotically stable by driving the line to a point near zero. likewise, ASMC and ASMFC could reduce the size of chatter as well as the control trouble without the demand to establish the system's upper set originally [8]. To achieve a stable system with minimum chatter while taking a short settling time, an SMFC approach with an achromatism function was presented to pretend an SMC's nonlinear input/ affair chart using a fuzzy conclusion approach applied to a language rule base [9]. In this study, a CSMC with SF and BF, as well as an ASMC with SF and BF, were developed and evaluated using a 2-link robot. To reduce the chatter in CSMC and ASMC, an achromatism function is used rather than a signum function in the spastic control section. Where, to exclude the drooling

miracle in CSMC a BF is used rather than a spastic control part. Also, CSMFC and ASMFC can exclude the drooling miracle with a lower settling time in comparison with CSMC with BF. Also, using ultramodern styles, SMFC with achromatism function and ASMFC with achromatism function have been designed to exclude the chatter problem and reduce settling time. What comes next is how this work is organized. The second segment describes a detailed model of a two-link robot manipulator. The third segment focuses on the construction of multiple controllers with two separate types of functions. The fourth segments show the outcomes of the controller adjustment. The fifth segment ends with some findings.

2. MATHEMATICAL MODEL OF 2-LINK ROBOT MANIPULATOR

A robotic rigger can carry out a variety of tasks in a variety of domains. Robotic systems can be used in dangerous environments for security and in industrial settings to construct machines and automation [10, 11]. Figure 1 depicts the 2-link robot in more detail.

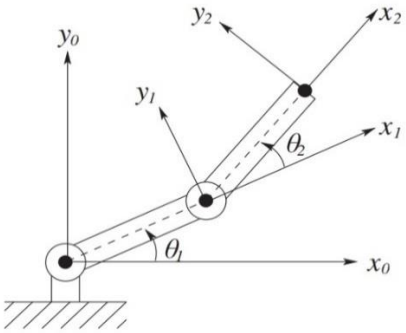

Figure 1. 2-link robot arm

Lagrange dynamics [12] can be used to obtain the manipulator's dynamics. Refer to Appendix A for manipulator dynamics, which are described in standard form [11]:

$$M(\theta)\ddot{\theta} + C\left(\theta,\dot{\theta}\right) + G(\theta) = \tau \tag{1}$$

where, θ, $\dot{\theta}$, $\ddot{\theta}$ indicate joint angular position, velocity, and acceleration vectors have dimension 2×1; τ represents a torque vector with dimensions of 2×1; $M(\theta)$ indicates a 2×2 inertia matrix; $C\left(\theta,\dot{\theta}\right)$ the diagram depicts Carioles central force (Ca.) forces in a 2×2 grid; $G(\theta)$ It is a 2×1 indicates a gravitational vector.

The variables in Eq. (1) are clarified as follows:

$$M(\theta) = \begin{bmatrix} M_{11} & M_{12} \\ M_{21} & M_{22} \end{bmatrix}$$

where,

$M_{11} = (m_1 + m_2)l_1^2 + m_2 l_2^2 + 2m_2 l_1 l_2 \cos(\theta_2)$;
$M_{12} = m_2 l_2^2 + 2m_2 l_1 l_2 \cos(\theta_2)$;
$M_{12} = M_{21}$;
$M_{22} = m_2 l_2^2$.

C indicates the Ca. and centrifugal matrix which is given by:

$C = \begin{bmatrix} C_1 \\ C_2 \end{bmatrix}$,
$C_1 = m_2 l_1 l_2 \sin(\theta_2)\dot{\theta}_2^2 - 2m_2 l_1 l_2 \sin(\theta_2)\,\dot{\theta}_1\dot{\theta}_2$;
$C_2 = m_2 l_1 l_2 \sin(\theta_2)\,\dot{\theta}_2^2$.

G represents the gravitational vector and represented by:

$G = \begin{bmatrix} G_1 \\ G_2 \end{bmatrix}$;
$G_1 = m_2 l_2 cos(\theta_1 + \theta_2) + (m_1 + m_2) l_1 g cos(\theta_1)$;
$G_2 = m_2 l_2 cos(\theta_1 + \theta_2)$;
$\tau = \begin{bmatrix} \tau_1 \\ \tau_2 \end{bmatrix}$.

As stated in this research, an additional claim about the current status is:

$$\theta_1 = x_1 + \theta_{1d};\ \theta_2 = x_2 + \theta_{2d} \tag{2}$$

where, θ_{1d} and θ_{2d} are the desirable angles for joint-1 and joint-2, respectively.

The Robot's Model can be rewritten as follows:

$$\begin{aligned} \dot{x}_1 &= x_2 \\ \dot{x}_2 &= -M(\theta)^{-1}(C\left(\theta,\dot{\theta}\right) + G(\theta) + \tau + \delta(x,u)) \end{aligned} \tag{3}$$

Eq. (3) could be updated in the following format:

$$\begin{aligned} \dot{x}_1 &= x_2 \\ \dot{x}_2 &= F + u + \delta \end{aligned} \tag{4}$$

The characters in Eq. (4) refer to the next equations:

$$x_1 = \begin{bmatrix} x_1 \\ x_2 \end{bmatrix},\ x_2 = \begin{bmatrix} x_3 \\ x_4 \end{bmatrix} \tag{5}$$

$$F = \begin{bmatrix} F_1 \\ F_2 \end{bmatrix} = -M(\theta)^{-1}(C\left(\theta,\dot{\theta}\right)\dot{\theta} + G(\theta)) \tag{6}$$

$$u = \begin{bmatrix} u_1 \\ u_2 \end{bmatrix} = -M(\theta)^{-1}\tau \tag{7}$$

$$\delta = \begin{bmatrix} \delta_1 \\ \delta_2 \end{bmatrix} = \Delta F + F_c + D(t) \tag{8}$$

where, ΔF=10% F, is pu for variables F.

In both joints, the friction coefficient of Coulomb (cf) is $Fc = \begin{bmatrix} F_{c1} \\ F_{c2} \end{bmatrix}$ and $D(t) = \begin{bmatrix} d_1(t) \\ d_2(t) \end{bmatrix}$indicates the ed.

The system's behavior can be represented as:

$$\begin{aligned} \dot{x}_1 &= x_3 \\ \dot{x}_2 &= x_4 \\ \dot{x}_3 &= F_1 + u_1 + \delta_1 \\ \dot{x}_4 &= F_2 + u_2 + \delta_2 \end{aligned} \tag{9}$$

The terms δ_1 and δ_2 denote joint 1 and 2 disturbances, respectively. Two minor problems occur with the CSMC's chatter and gain parameters for attitude control. As a result, while replacing the SF is an effective noise resolution technique, ASMC has been recognized as a great approach to reduce the gain component for optimal control. In a comparable manner, BF-based ASMC applies to both of the aforementioned entities. This study uses two definitions of BF [7, 13].

2.1 Barrier function

Definition [7]: The BF is a nonstop function f: x∈[−ε, ε]→$l_b(x)$∈[b, ∞] that almost rises at (0, ε).

·lim |x|→ε$l_b(x)$=+∞.

·$l_b(x)$ has an initial value of 0, and $l_b(0)=b\geq 0$.
There are two classifications of BF.
1-Positive-definite BF (PBF):

$$l_{pb}(x)=\frac{\varepsilon F}{\varepsilon-|x|}, \text{ i.e., } l_{pb}(0)=F>0 \quad (10)$$

2-PositiveSemi-definite BF (PSBF):

$$l_{psb}(x)=\frac{|x|}{\varepsilon-|x|}, \text{ i.e., } l_{psb}(0)=0 \quad (11)$$

The defined function in Eq. (10) and Eq. (11) gives adaptive and classical gains based on PBF and PSBF. Thus, when $\varepsilon\rightarrow 0$, $K\rightarrow 0$. Still, if the state is close to the origin. If $\frac{|x|}{\varepsilon}<1$, then $K\approx\frac{|x|}{\varepsilon}$, indicating that state x is converging to zero [13]. The PBF $l_{psb}(x)$ chosen and will be utilized in this study to outcome the 2-link robot.

3. THE DESIGNING OF THE SLIDING MODE CONTROLLER

The SMC is an ideal controller designed to provide reliability in the face of an examination, but it is vulnerable to fluctuations of limit ability and amplitude known as the chatter issue, which is a renowned topic in SMC. Several techniques for avoiding chatter are offered, including ASMC and the boundary subcaste system [11]. The concept of SMC began in nineteenth-century structure and equilibrium studies before emerging as an engineering topic in the late 1950s [14].

3.1 The designing of CSMC

Figure 2 displays the CSMC's two phases: the reaching phase (RP) and the sliding phase (SP). Control procedures can be separated into two types: nominally control (NC) and discontinuity control (DC). The DC informs the system's state line to follow the ss. till it arrives the beginning, whereas the SMC's NC directs the state line from the starting point to the ss.'s direction [15-17].

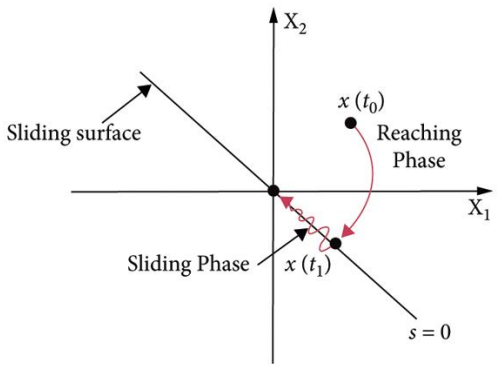

Figure 2. RP and SP of CSMC

The sliding surface can be written as [11, 14, 15]:

$$u_{dis}=-k(x)sign(s) \quad (12)$$

$$s=\lambda e+\dot{e}=0 \quad (13)$$

here, lambda (λ) is the slope and it is>0.

Let us assume that x_1 is e and x_2 is $\dot{e}$, ss. re-written as:

$$s=\lambda x_1+x_2=0 \quad (14)$$

where, λ=1, the ss. is:

$$s=x_1+x_2=0 \quad (15)$$

The control law as follows:

$$u=u_n+u_{dis} \quad (16)$$

where, u_n is the NC, and the u_{dis} DC [12, 13].
The DC is defined as below:

$$u_{dis}=-k(x)sat(s) \quad (17)$$

where, $k(x)$ is a discontinuity gain that integrates all pu, ed, and cf, and sat(s) is an SF, as specified in Eq. (18):

$$sat(s,\varphi)=\begin{cases} sign(s) & if|s|>\varphi \\ \frac{s}{\varphi} & if|s|\leq\varphi \end{cases} \quad (18)$$

where, phi (φ) is the width of SF as seen in Figure 3.

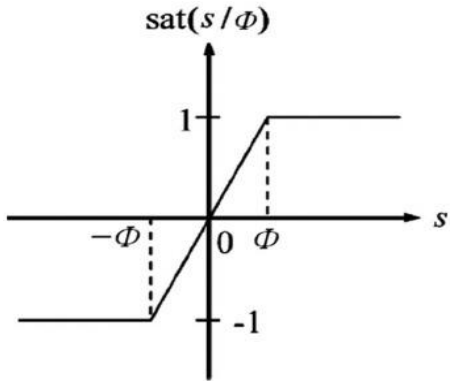

Figure 3. The sat(s) function [18]

where,

$$sign(s)=\begin{cases} 1 & \text{if } s>0 \\ -1 & \text{if } s<0 \\ \in[-1.1] & \text{if } s=0 \end{cases} \quad (19)$$

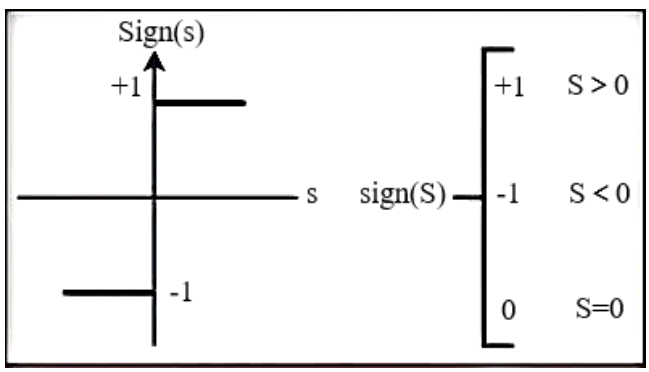

Figure 4. The sign(s) function [18]

Eq. (19) is also shown in Figure 4. As a consequence, the formula for the control action appears under [19]:

$$u = u_n - k(x).sat(s, \varphi) \quad (20)$$

And replace DC in Eq. (15) with BF then:

$$u = u_n - \frac{s}{|\eta - |s||} \quad (21)$$

The ss. can be stated as follows:

$$s_1 = \lambda x_1 + x_3 \quad (22)$$

$$s_2 = \lambda x_2 + x_4 \quad (23)$$

where, x_1 and x_2 indicate errors of links 1 and 2, and x_3 and x_4 indicate the derivative of error of links 1 and 2, respectively.

Let λ=1, then, Eq. (22) and Eq. (23) are recast in a new manner:

$$s_1 = x_1 + x_3 \quad (24)$$

$$s_2 = x_2 + x_4 \quad (25)$$

The gain $k(x)$ the value is determined by extrapolating a particular situation:

$$\dot{s}<0 \quad (26)$$

where, $s=\begin{bmatrix} s_1 \\ s_2 \end{bmatrix}$.

By including Eq. (15) in Eq. (26):

$$x_1 + x_2 < 0$$

Using Eq. (4) and Eq. (8):

$$k(x)>|\delta|$$

$$k(x)=k_o\ (\Delta F+D) \quad (27)$$

where, k_o>0.

$$k(x)=\begin{bmatrix} k_1(x) \\ k_2(x) \end{bmatrix} \quad (28)$$

where, $k_1(x)$ is the control action gain for link one, while $k_2(x)$ is the control action gain for link two. If the gain values of each link are discovered and entered into Eq. (16), torques can be calculated as follows:

$$\tau_1=M_{11}\ u_1+M_{12}\ u_2 \quad (29)$$

$$\tau_2=M_{21}u_1+M_{22}\ u_2 \quad (30)$$

3.2 Design of fuzzy logic controller (FLC)

FLC eliminates the need for sophisticated mathematical models, resulting in considerably simpler and more robust control principles [18].

FLC directly handles input and output variable inaccuracy by describing them in terms of language using fuzzy integer numbers and fuzzy sets [19, 20].

Within systems, FLCs are implemented to infuse the controller with intelligence, integrating human decision-making and expertise into the operational processes. The representation of relationships between input and output involves the utilization of sets of linguistic rules or relational expressions. In recent decades, researchers have shown considerable interest in FLC, employing it as a distinctive or competitive control strategy across diverse plant applications [21-23].

3.3 Membership function (MF)

MF fuzzy class functions serve an important role in identifying how many items are part of a fuzzy set within colored variables. These functions describe the degree to which an element resembles a given fuzzy set. Class functions display colorful shapes such as triangular, etc., as described in references [24, 25]. The triangular class functions employed in this paper is highlighted by their elegant simplicity. Three parameters, a, b, and c, are used to characterize the class function $\mu_A(x)$ for each value x (see Figure 5). The values of these factors are derived from professional knowledge [26].

The c membership function $\mu_A(x)$ has been represented by:

$$\mu_A(x) = \begin{Bmatrix} 0 & \text{if} \quad x \le a \\ \frac{x-a}{b-a} & \text{if} \quad a \le x \le b \\ \frac{c-x}{c-b} & \text{if} \quad b \le x \le c \\ 0 & \text{if} \quad x \ge c \end{Bmatrix} \quad (31)$$

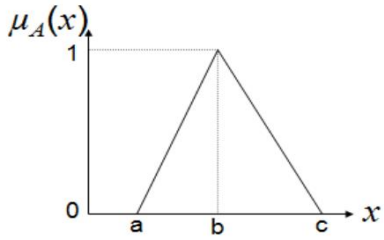

Figure 5. The Gaussian membership function membership function [26]

3.4 Structure of FLC

The structure of the fuzzy controller, illustrated in Figure 6, consists of essential components, namely fuzzification, inference mechanism, rule basis, and defuzzification.

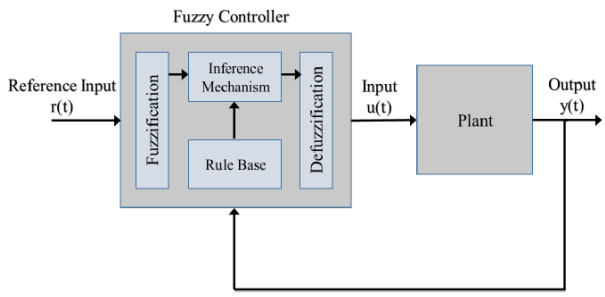

Figure 6. The anatomy of the fuzzy controller [22, 24, 27]

3.4.1 The fuzzification

During this stage, input data is converted into verbal variables, whose values are decided by the input class functions.

This metamorphosis allows for the effective activation and perpetration of rules in the conclusion process.

3.4.2 The rule-base

An approach to decision-making that emulates mortal cognitive processes and includes a definition of fuzzy class functions for each control variable. This system also outlines the criteria for expressing control objects through verbal variables.

3.4.3 The inference mechanism (Inference engine)

The Inference Mechanism method generates fuzzy conclusions by applying the fuzzy rules in the rule base. The conclusion medium consists of two abecedarian tasks: (1) determining the amount to which each rule is appropriate for the current situation defined by inputs u_i, where i=1, 2, and n; this assignment is commonly referred to as "identifying," and (2) getting a decision based on the current u_i inputs and the knowledge embedded in the rule base; this task is referred to as "conclusion step."

3.4.4 The defuzzification

The verbal variables that are presumed are converted into numerical values. Defuzzification accepts as input the class (confidence) of inferred fuzzy sets derived from premise rules and returns a crisp integer. The three main defuzzification procedures used for estimating fuzzy sets are the Center of Gravity (COG), etc., (22, 24, 27). There are two types of fuzzy conclusion systems, the first of which is commonly used: Mamdani's fuzzy conclusion system. The Takagi-Sugeno-Kang (T.S.K) fashion is an alternative. This system is also called the T.S.K system. The issue of fuzzy rules is the primary difference between the two systems. As a rule repercussions, T.S.K fuzzy systems make use of straight functions of input variables, whereas Mamdani fuzzy systems employ fuzzy sets [28].

3.5 Design of sliding mode fuzzy controller (SMFC)

SMC has an unwanted noise behavior called chatter. As a result, the current study focuses on merging fuzzy understanding with conventional sliding mode controllers to create an innovative design known as the CSMFC, which has superior performance (short settling time, rapid reaction, and no oscillation). Our major goal is to create an effective control rule for the system's activities that follows the reference circles depicted in Table 1.

The CSMFC's organization is divided into two segments, as detailed below:

1: The CSMC: This component takes error (e) as an input and outputs u_s [20].

2: The fuzzy controller: This component only has one input (s) and one output (u_{fuzzy}). The input (s) is derived from the output of the sliding mode controller [20]. The fuzzy controller's membership functions are depicted in Figure 5 below:

Table 1. Table of fuzzy rules for Figure 7 and Figure 8 in CSMFC and ASMFC systems [20]

S	*nb*	*ns*	*z*	*ps*	*pb*
***U**f*	*pb*	*ps*	*ze*	*ns*	*nb*

where, *nb*, *ns*, *z*, *ps*, and *pb* are antecedent fuzzy set linguistic concepts as presented in Figures 7 and 8. They stand for negative big, negative small, zero, positive small, and positive big, in that order. As demonstrated below, a generic form may be used to define the fuzzy rules [20]:

$$\text{If } S \text{ is } A_i, \text{then } U_f \text{ is } B_i, i = 1, \dots, 5 \tag{32}$$

where, A_i represents the fuzzy triangle-shaped integer and B_i represents the fuzzy square-shaped number singleton [20].

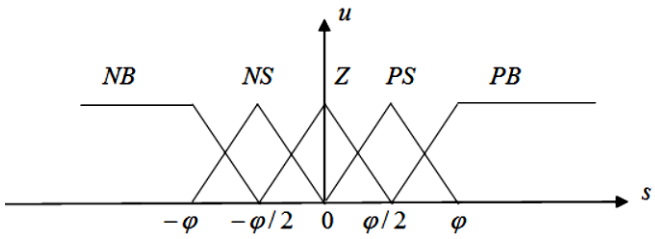

Figure 7. The input membership [20]

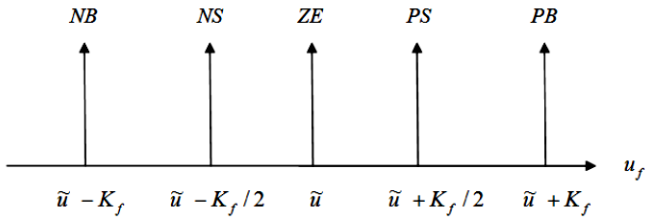

Figure 8. The output membership function [20]

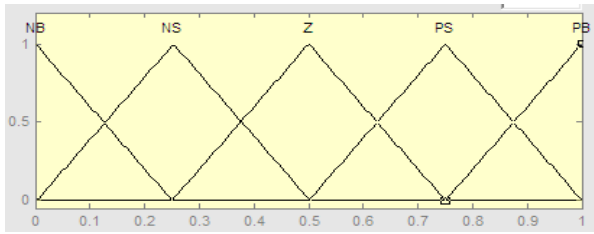

Figure 9. The membership function of the fuzzy controller [20]

From Figure 6 and Figure 9, it can be concluded that for the SMFC:

$$u = \tilde{u} - k_f . sig(\frac{s}{\varphi}) \tag{33}$$

$$sig(a) = \begin{cases} +1 & \text{if} \quad a \geq 1 \\ a & \text{if} \quad -1 < a < 1 \\ -1 & \text{if} \quad a \leq -1 \end{cases} \tag{34}$$

The control signals for the SMFC (Eq. (33)) and the ASMC (Eq. (20)) are similar. The membership function for the input and output of the fuzzy controller component of the SMFC design can be established via the modified SMC. To replace the fuzzy output center $\tilde{u}$ and gain k_f in Eq. (33) for the CSMFC, use u_n and k from Eq. (20) for the modified SMC. As a result, the fuzzy controller component of the SMFC may be guaranteed to be completely stable and lasting. As a result, the SMFC's whole controller will be described as [20]:

$$u_{total} = u_{sliding} + u_{fuzzy} \tag{35}$$

where, $u_{sliding}$ is defined in Eq. (20). So, Eq. (35) can be re-written as:

$$u_{total} = u_n + k.sat(s/\varphi) + u_{fuzzy} \tag{36}$$

3.6 The designing of ASMC

The ASMC's architecture is as follows:

$$u(s.t) = -k(t)\ sign(x.t) \tag{37}$$

where, $k(t)$ represents the gain that varies with time, and it may be expressed as in reference [7].

As previously stated, the BF in Eq. (37) has been replaced with the SF to reduce chatter.

$$\dot{k}(t) = \{^{\rho.|s(x.t)|.sign(|s(x.t)|)-\epsilon),\quad \text{if } k > \mu}_{\mu,\quad\quad\quad\quad\quad\quad\quad\quad \text{if } k \le \mu\}} \tag{38}$$

where, ρ>0, $k(t)$ increases or decreases, μ and ϵ are positive constants to be selected. The guidelines (Eq. (38)) state that the amount of unpredictability (the higher and smaller bounds) is not included in the calculation of the minimally acceptable gain (adaptive gain), even though the uncertainty had to be computed in CSMC, as indicated in Eqs. (26)-(28).

3.7 The designing of ASMFC

This section presents an organized approach to building a stable ASMFC, in addition, the control rule and measuring adaption techniques guarantee that tracked error is exactly confined to any minor amount of the points around the origin. Also, every signal in the closed-loop system has been proven to be limited [19].

The ASMFC's whole controller will be detailed as follows: Combine Eq. (35) and Eq. (36) with replacing sign function with SF.

$$u_{total} = u_{eq} + k(t).sat(s/\varphi) + u_{fuzzy} \tag{39}$$

4. THE SIMULATION RESULTS

In this work, CSMC and ASMC were designed depending on using a SF and a BF, also, SMFC and ASMFC were developed based on the use of a SF manipulator despite the effects of uncertainty, Coulomb friction, and disturbance on each link. These four methods were simulated with the Matlab2018a/Simulink program to show the activity of the proposed methods. The system variables are listed in Table 2. where, the initial conditions are $x_1(0) = \frac{\pi}{8}(rad.)$, $x_2(0) = \frac{\pi}{16}(rad.)$, $x_3(0)$=0 (*rad./sec.*), and $x_4(0)$=0 (*rad./sec.*).

Table 2. The parameters of 2-link robot

Parameter	Description	Value (unit)
l_1	The length of link 1	0.7 (m)
l_2	The length of link 2	0.3 (m)
m_1	The mass of link 1	0.2 (kg)
m_2	The mass of link 2	0.1 (kg)
θ_1 desired	Theta desirable of link 1	$\frac{\pi}{3}(rad.)$
θ_2 desired	Theta desirable of link 2	$\frac{\pi}{2}(rad.)$
d_1	Disturbance of link 1	0.1 (N.m.)
d_2	Disturbance of link 2	0.1 (N.m.)
F_{c1}	Coulomb frictions of link 1	0.031 (N.m.)
F_{c1}	Coulomb frictions of link 2	0.052 (N.m.)
φ	Width of boundary layer	0.9
ε	Eta for BF	0.09

The values of the ASMC control law coefficients in Eq. (37) are given below: ρ_1=20, ρ_2=19, ϵ_1=ϵ_2=0.002, μ_1=30, μ_2=29, $k_1(0)$=20, $k_2(0)$=19.

Figures 10 and 11 demonstrate the development of various states from their beginning positions: $x_1(0) = \frac{\pi}{8}$, $x_2(0) = \frac{\pi}{16}$, $x_3(0)$=0 and $x_4(0)$=0 for joints 1 and 2, till equilibrium is achieved. As a result, the system is expected to be asymptotically stable owing to the combination of too-close neighbors to zero (the intended location), as shown in Figures 12 and 13. This indicates that the error and its derivative are zero or close to zero, resulting in the two-link robot's accurate following movement, as illustrated in Figures 14-17.

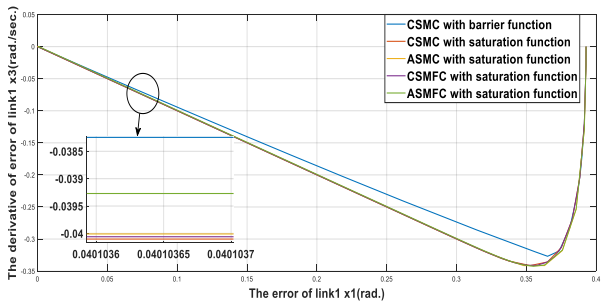

Figure 10. The trajectory of joint-1 for different controllers

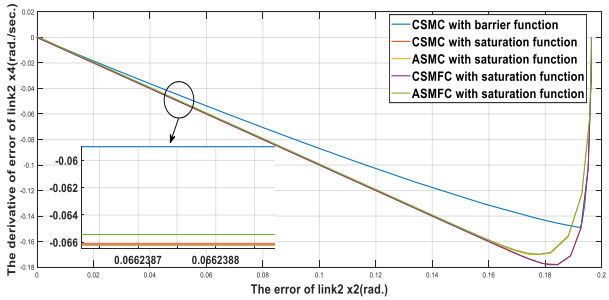

Figure 11. The trajectory of joint-2 for different controllers

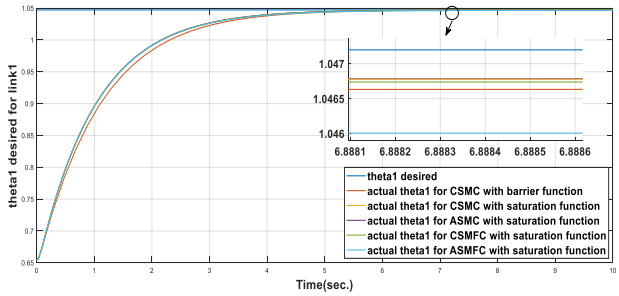

Figure 12. The performance of tracking between θ_1 and θ_{d1} for different controllers

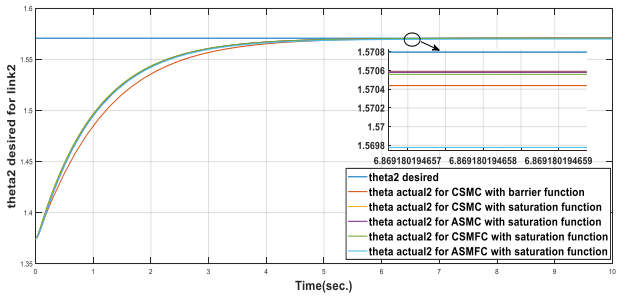

Figure 13. The performance of tracking between θ_1 and θ_{d2} for different controllers

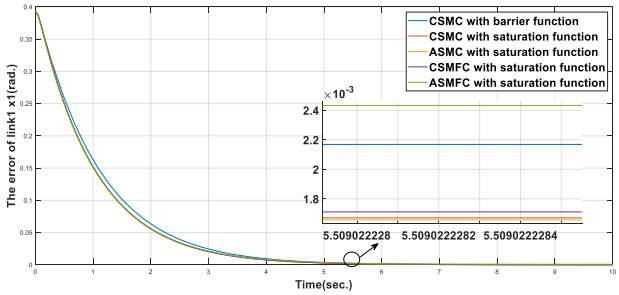

Figure 14. The x_1 (rad.) for different controllers

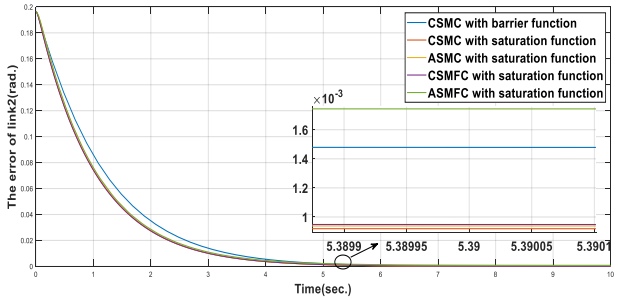

Figure 15. The x_2 (rad.) for different controllers

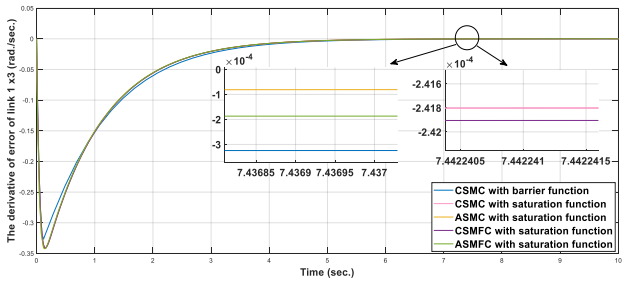

Figure 16. The x_3 (rad./sec.) for different controllers

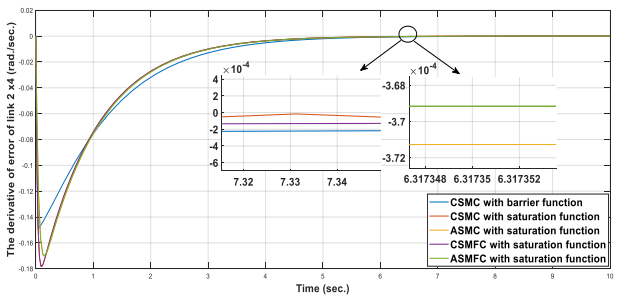

Figure 17. The x_4 (rad./sec.) for different controllers

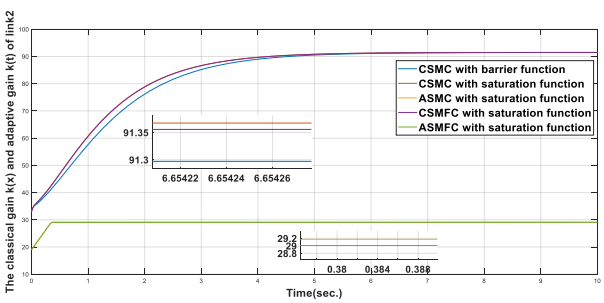

Figure 18. The k(t) and k(x) of joint-1 for different controllers

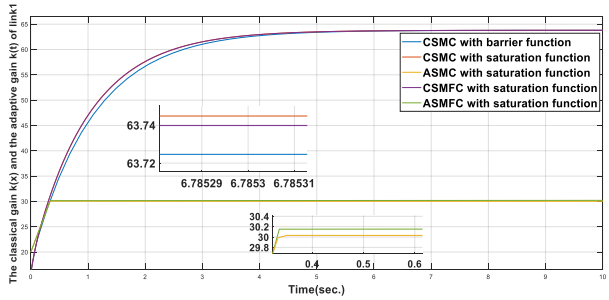

Figure 19. The k(t) and k(x) of joint-2 for different controllers

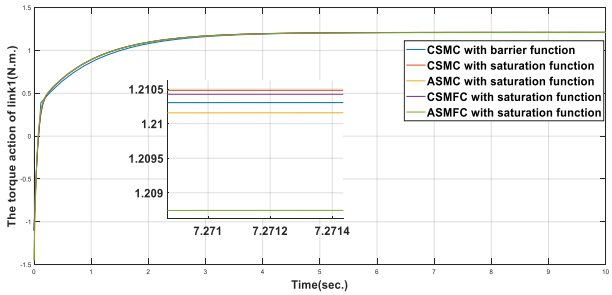

Figure 20. The τ_1 (N.m.) for different controllers

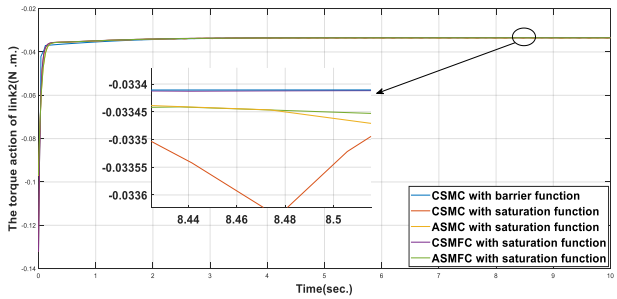

Figure 21. The τ_2 (N.m.) for different controllers

Figure 18 and Figure 19 demonstrate the gain controller of each joint for CSMC with SF and with BF, ASMC with SF, CSMFC with SF, and ASMFC with SF, respectively. CSMC with SF and with BF provides a high level, resulting in maximum effort torque action and chatter is reduced to near zero when using CSMC with a BF, despite CSMC suffering from chatter even when using boundary layer SF, as shown in Figure 20 and Figure 21. In ASMC with SF it delivers a low level, resulting in a minimal effort torque action and it suffers from chatter, as shown in Figure 20 and Figure 21. Where the chatter decreased approximately to zero in applying ASMFC and CSMFC with SF as shown in Figure 20 and Figure 21.

Table 3 listed the settling time, the magnitude of chatter, and steady-state gain for joint-1 and joint-2 while applying the CSMC with SF and with BF, ASMC with SF, CSMFC with SF, and ASMFC with SF, respectively and it was discovered that the chatter was reduced to a lower acceptable level when using the CSMC with the BF and the ASMC was utilized with the SF the chatter dropped to a more bearable level, and the settling time was shortened. When using the ASMFC and CSMFC with SF, the noise lowered to a more manageable level, and the settling time was less when using the CSMFC with SF.

Table 3. The simulation results

Content	CSMC with BF	CSMC with SF	ASMC with SF	CSMFC with SF	ASMFC with SF
ST (sec.)	4.3	4	4	3.7	3.9
MOC B-B (N. m)	≈ 0	0.00019	0.00013	=0	=0
SSOG J-1	63.79	63.79	30.02	63.78	30.21
SSOG J-2	91.49	91.49	29.15	91.47	29.06
RT (sec.)	1.5	1.5	0.5	1.5	0.5

Where ST represents settling time, MOC B-B represents the magnitude of chatter beak to beak, SSOG J-1 represents the steady state of gain for joint-1 and SSOG J-2 1 represents the steady state of gain for joint-2, RT represents rise time respectively.

5. CONCLUSIONS

Despite nonlinearity in the actuator, uncertainty in parameters, friction, and external disturbance, the fuzzy controller with SF approach is utilized to develop a robust sliding mode controller for a 2-link robot. CSMFC and ASMFC with SF are used to increase CSMC and ASMC performance by lowering the controller gain to a lower accessible level, resulting in a lower control input, as shown in Figures 16 and 17. Unlike CSMFC, which needs an understanding of the limits of unpredictability, ASMC does not, and in situations when the limit of unpredictability is unknown, the motion of the 2-link robot influences the computations of adaptive gain, causing it to follow the correct trajectory. The simulation results demonstrated the efficacy of our suggested strategy for reducing chatter, while as a result, asymptotic stability was attained as seen in Figure 10 and Figure 11. On the other hand, CSMFC with SF gives a lower settling time followed by ASMFC with SF which gives a small settling time as the worst one is CSMC with BF as shown in Figure 12, Figure 13, and Table 3. As seen in Figure 12, Figure 13 and Table 3, firstly, ASMFC with SF guarantees zero magnitudes of chatter in comparison with CSMC and ASMC with SF which has a small magnitude of chatter. Secondly, CSMFC with SF has a zero magnitude of chatter. Finally, CSMC with BF also has a zero magnitude of chatter. On the other hand, CSMFC with SF has more stability and lower settling time. The efficiency of the proposed CSMFC and ASMFC were proved and confirmed using simulation results for different model parameters with low uncertainty in model parameters and with the presence of nonlinearity, frictions, and disturbances. The CSMFC reduces chattering and the effects of nonlinearities regardless of the presence of uncertainty, disturbance, and friction in the suggested systems. This is the main feature of the CSMFC, as established in Chapter Four. Also, it is demonstrated in simulation results, a comparison between CSMFC and CSMC as well as a comparison between ASMFC and ASMC.

REFERENCES

[1] Ajwad, S.A., Islam, R.U., Azam, M.R., Ullah, M.I., Iqbal, J. (2016). Sliding mode control of rigid-link anthropomorphic robotic arm. In 2016 2nd International Conference on Robotics and Artificial Intelligence (ICRAI), Rawalpindi, Pakistan, pp. 75-80. https://doi.org/10.1109/ICRAI.2016.7791232

[2] Azizi, A., Mobki, H. (2021). Applied mechatronics: Designing a sliding mode controller for active suspension system. Complexity, 2021(1): 6626842. https://doi.org/10.1155/2021/6626842

[3] Jedda, O., Ghabi, J., Douik, A. (2017). Sliding mode control of an inverted pendulum. Applications of Sliding Mode Control, 105-118. https://doi.org/10.1007/978-981-10-2374-3_6

[4] Fulwani, D., Bandyopadhyay, B. (2013). Design of sliding mode controller with actuator saturation. In Advances in Sliding Mode Control: Concept, Theory and Implementation, pp. 207-219. https://doi.org/10.1007/978-3-642-36986-5_10

[5] Elkhateeb, N.A., Badr, R.I. (2017). Novel PID tracking controller for 2DOF robotic manipulator system based on artificial bee colony algorithm. Electrical, Control and Communication Engineering, 13(1): 55-62. https://doi.org/10.1515/ecce-2017-0008

[6] Azizi, A., Mobki, H. (2021). Applied mechatronics: Designing a sliding mode controller for active suspension system. Complexity, 2021(1): 6626842. https://doi.org/10.1155/2021/6626842

[7] Obeid, H., Fridman, L.M., Laghrouche, S., Harmouche, M. (2018). Barrier function-based adaptive sliding mode control. Automatica, 93: 540-544. https://doi.org/10.1016/j.automatica.2018.03.078

[8] Samanfar, A., Shakarami, M.R., Soltani Zamani, J., Rokrok, E. (2022). Adaptive sliding mode control for multi-machine power systems under normal and faulted conditions. Scientia Iranica, 29(5): 2526-2536. https://doi.org/10.24200/sci.2020.55717.4371

[9] Dotoli, M., Maione, B., Naso, D. (2002). Fuzzy sliding mode controllers synthesis through genetic optimization. Advances in Computational Intelligence and Learning: Methods and Applications, 331-341. https://doi.org/10.1007/978-94-010-0324-7_23

[10] Mobayen, S., Tchier, F., Ragoub, L. (2017). Design of an adaptive tracker for n-link rigid robotic manipulators based on super-twisting global nonlinear sliding mode control. International Journal of Systems Science, 48(9): 1990-2002. https://doi.org/10.1080/00207721.2017.1299812

[11] Al-hadithy, D., Hammoudi, A. (2020). Two-link robot through strong and stable adaptive sliding mode controller. In 2020 13th International Conference on Developments in eSystems Engineering (DeSE), Liverpool, United Kingdom, pp. 121-127. https://doi.org/10.1109/DeSE51703.2020.9450762

[12] Lewis, F.L., Dawson, D.M., Abdallah, C.T. (2003). Robot Manipulator Control: Theory and Practice. CRC Press. https://doi.org/10.1201/9780203026953

[13] Shtessel, Y., Edwards, C., Fridman, L., Levant, A. (2014). Sliding Mode Control and Observation (Vol. 10). New York: Springer New York. https://doi.org/10.1007/978-0-8176-4893-0_8

[14] Tu'ma, D.H., Hamoudi, A.K. (2020). Performance of 2-

link robot by utilizing adaptive sliding mode controller. Journal of Engineering, 26(12): 44-65. https://doi.org/10.31026/j.eng.2020.12.03.
[15] Hamoudi, A.K., Rahman, N.O.A. (2017). Design an integral sliding mode controller for a nonlinear system. Al-Khwarizmi Engineering Journal, 13(1): 138-147. https://doi.org /10.22153/kej.2017.09.003
[16] Tohma, D.H., Hamoudi, A.K. (2021). Design of adaptive sliding mode controller for uncertain pendulum system. Engineering and Technology Journal, 39(3A): 355-369. https://doi.org/10.30684/etj.v39i3A.1546
[17] Badri, A.S. (2014). Integral sliding mode controller design for electronic throttle valve. Doctoral dissertation, M.Sc. Thesis, University of Technology, Baghdad, Iraq. https://doi.org/10.30684/etj.2017.127327
[18] Alli, H., Yakut, O. (2005). Fuzzy sliding-mode control of structures. Engineering Structures, 27(2): 277-284. https://doi.org/10.1016/j.engstruct.2004.10.007
[19] Bououden, S., Chadli, M., Karimi, H.R. (2013). Fuzzy sliding mode controller design using Takagi-Sugeno modelled nonlinear systems. Mathematical Problems in Engineering, 2013(1): 734094. https://doi.org/10.1155/2013/734094
[20] Hamoudi, A.K. (2016). Design and simulation of sliding mode fuzzy controller for nonlinear system. Journal of Engineering, 22(3): 66-76. https:/doi.org/10.31026/j.eng.2016.03.05
[21] AL-Tameemi, D.W.I.M., Hadi, M.W.M.H. (2015). Modeling and control of 5250 lab-volt 5 DoF robot manipulator. https://uotechnology.edu.iq/ijcccse_journal/no.2.2015/abstracts/5-Wathek_Waeel.pdf.
[22] Raheem, F.A., Midhat, B.F., Mohammed, H.S. (2018). PID and fuzzy logic controller design for balancing robot stabilization. Iraqi Journal of Computers, Communications, Control and Systems Engineering, 18(1): 1-10. https://doi.org/10.33103/uot.ijccce.18.1.1
[23] Kadhim, H.M., Oglah, A.A. (2020). Interval type-2 and type-1 fuzzy logic controllers for congestion avoidance in Internet routers. IOP Conference Series: Materials Science and Engineering, 881(1): 012135. https://doi.org/10.1088/1757-899X/881/1/012135
[24] Passino, K.M. (1998). Fuzzy Control. Addition Wesley.
[25] Barman, M., Chaudhury, J.P. (2013). A framework for selection of membership function using fuzzy rule base system for the diagnosis of heart disease. International Journal of Information Technology and Computer Science, 5(11): 62-70. https://doi.org/10.5815/ijitcs.2013.11.07
[26] Yahia, N.B., Bellamine, N., Ghezala, H.B. (2012). Integrating fuzzy case-based reasoning and particle swarm optimization to support decision making. International Journal of Computer Science Issues, 9(3): 117.
[27] Wonohadidjojo, D.M., Kothapalli, G., Hassan, M.Y. (2013). Position control of electro-hydraulic actuator system using fuzzy logic controller optimized by particle swarm optimization. International Journal of Automation and Computing, 10: 181-193. https://doi.org/10.1007/s11633-013-0711-3
[28] Ghintab, S.S., Hassan, M.Y. (2014). Intelligent controller design of rehabilitation robot for lower limb movements. M.Sc. Thesis, University of Technology, Iraq.

APPENDIX A

The derivation of the Lagrange equation for 2-LRRM

The expressions describing the *x*- position and *y*-position of link 1 are provided by [23]:

$$x_1 = l_1 \cos(\theta_1) \tag{A1}$$

$$y_1 = l_1 \sin(\theta_1) \tag{A2}$$

Likewise, the equations representing the x-position and y-position of link 2 are provided by:

$$x_2 = l_1 \cos(\theta_1) + l_2 \cos(\theta_1 + \theta_2) \tag{A3}$$

$$y_2 = l_1 \sin(\theta_1) + l_2 \sin(\theta_1 + \theta_2) \tag{A4}$$

The differentiation of the *x* and *y* positions for link-1 and link-2 is expressed by the following equations:

$$\dot{x_1} = -l_1 \dot{\theta_1} \sin(\theta_1) \tag{A5}$$

$$\dot{y_1} = l_1 \dot{\theta_1} \cos(\theta_1) \tag{A6}$$

$$\dot{x_2} = -l_1 \dot{\theta_1} \sin(\theta_1) - l_2 \sin(\theta_1 + \theta_2) \tag{A7}$$

$$\dot{y_2} = l_1 \dot{\theta_1} \cos(\theta_1) + l_2 \cos(\theta_1 + \theta_2)\left(\dot{\theta_1} + \dot{\theta_2}\right) \tag{A8}$$

The kinetic energy is defined as:

$$KE = \frac{1}{2} m_1 {v_1}^2 + \frac{1}{2} m_2 {v_2}^2 \tag{A9}$$

where, v_1 and v_2 are the velocities for m_1 and m_2 respectively and can be calculated as:

$$v_1 = \sqrt{\dot{x_1}^2 + \dot{y_1}^2}, v_2 = \sqrt{\dot{x_2}^2 + \dot{y_2}^2} \tag{A10}$$

So the kinetic energy will be

$$KE = \frac{1}{2} m_1 (\dot{x_1}^2 + \dot{y_1}^2) + \frac{1}{2} m_2 (\dot{x_2}^2 + \dot{y_2}^2) \tag{A11}$$

$$\begin{aligned} KE = {} & \tfrac{1}{2} m_1 ((-l_1 \dot{\theta_1} \sin(\theta_1))^2 + (l_1 \dot{\theta_1} \cos(\theta_1))^2) \\ & + \tfrac{1}{2} m_2 ((-l_1 \dot{\theta_1} \sin(\theta_1) - l_2 \sin(\theta_1 + \theta_2)(\dot{\theta_1} + \dot{\theta_2}))^2 + (l_1 \dot{\theta_1} \cos(\theta_1) + l_2 \cos(\theta_1 + \theta_2)(\dot{\theta_1} + \dot{\theta_2}))^2) \end{aligned} \tag{A12}$$

$$\begin{aligned} KE = {} & \frac{1}{2} m_1 l_1^2 \dot{\theta_1}^2 sin^2(\theta_1) + \frac{1}{2} m_1 l_1^2 \dot{\theta_1}^2 cos^2(\theta_1) \\ & + \frac{1}{2} m_2 l_1^2 \dot{\theta_1}^2 sin^2(\theta_1) \\ & + m_2 l_1 l_2 \dot{\theta_1} \sin(\theta_1) \sin(\theta_1 + \theta_2)(\dot{\theta_1} + \dot{\theta_2}) \\ & + \tfrac{1}{2} m_2 l_2^2 sin^2(\theta_1 + \theta_2)(\dot{\theta_1} + \dot{\theta_2})^2 + \\ & \tfrac{1}{2} m_2 l_1^2 \dot{\theta_1}^2 cos^2(\theta_1) + m_2 l_1 l_2 \dot{\theta_1} \cos(\theta_1) \cos(\theta_1 + \theta_2)(\dot{\theta_1} + \dot{\theta_2}) + \tfrac{1}{2} m_2 l_2^2 cos^2(\theta_1 + \theta_2)(\dot{\theta_1} + \dot{\theta_2})^2 \end{aligned} \tag{A13}$$

$$KE = \frac{1}{2}(m_1 + m_2)l_1^2\dot{\theta_1}^2 + m_2 l_1 l_2 \dot{\theta_1}(\sin(\theta_1)\sin(\theta_1+\theta_2) + \cos(\theta_1)\cos(\theta_1+\theta_2)) + m_2 l_1 l_2 \dot{\theta_1}\dot{\theta_2}(\sin(\theta_1)\sin(\theta_1+\theta_2)\cos(\theta_1)\cos(\theta_1+\theta_2) + \frac{1}{2} m_2 l_2^2 \dot{\theta_1}^2\left(sin^2(\theta_1+\theta_2) + cos^2(\theta_1+\theta_2)\right) + m_2 l_2^2 \dot{\theta_1}^2\dot{\theta_2}^2\left(sin^2(\theta_1+\theta_2) + cos^2(\theta_1+\theta_2)\right) + \frac{1}{2} m_2 l_2^2 \dot{\theta_2}^2\left(sin^2(\theta_1+\theta_2) + cos^2(\theta_1+\theta_2)\right) \quad (A14)$$

$$KE = (\frac{1}{2}(m_1 + m_2)l_1^2 + m_2 l_1 l_2 \cos(\theta_2) + \frac{1}{2} m_2 l_2^2)\dot{\theta_1}^2 + (m_2 l_1 l_2 \cos(\theta_2) + \frac{1}{2} m_2 l_2^2)\dot{\theta_1}^2\dot{\theta_2}^2 + \frac{1}{2} m_2 l_2^2 \dot{\theta_2}^2 \quad (A15)$$

And the potential energy can be written as:

$$PE = \sum_{i=1}^{2} m_i\, g h_i(\theta) \quad (A16)$$

$$PE = m_1 g l_1 \sin(\theta_1) + m_2 g(l_1 \sin(\theta_1) + l_2 \sin(\theta_1+\theta_2)) \quad (A17)$$

$$PE = (m_1 + m_2) g l_1 \sin(\theta_1) + m_2 g l_2 \sin(\theta_1+\theta_2) \quad (A18)$$

Following the principles of Lagrange Dynamics, we construct the Lagrangian, defined as:

$$L = KE - PE \quad (A19)$$

$$L = (\frac{1}{2}(m_1+m_2)l_1^2 + m_2 l_1 l_2 \cos(\theta_2) + \frac{1}{2} m_2 l_2^2)\dot{\theta_1}^2 + (m_2 l_1 l_2 \cos(\theta_2) + \frac{1}{2} m_2 l_2^2)\dot{\theta_1}^2\dot{\theta_2}^2 + \frac{1}{2} m_2 l_2^2 \dot{\theta_2}^2 - (m_1+m_2) g l_1 \sin(\theta_1) - m_2 g l_2 \sin(\theta_1+\theta_2) \quad (A20)$$

The Euler Lagrange Equation is given by:

$$\frac{d}{dt}\left[\frac{\partial l}{\partial \dot{\theta}_i}\right] - \frac{\partial L}{\partial \theta_i} = F\theta_i \quad (A21)$$

where, $F\theta_i$ is the torque applied to the i'th link.

$$\frac{\partial L}{\partial \dot{\theta_1}} = ((m_1 + m_2)l_1^2 + 2m_2 l_1 l_2 \cos(\theta_2) + m_2 l_2^2)\dot{\theta_1} + (m_2 l_1 l_2 \cos(\theta_2) + m_2 l_2^2)\dot{\theta_2} \quad (A22)$$

$$\frac{d}{dt}\left(\frac{\partial l}{\partial \dot{\theta_1}}\right) = ((m_1 + m_2)l_1^2 + 2m_2 l_1 l_2 \cos(\theta_2) + m_2 l_2^2)\ddot{\theta_1} - 2m_2 l_1 l_2 \dot{\theta_1}\dot{\theta_2}\sin(\theta_2) + (m_2 l_1 l_2 \cos(\theta_2) + m_2 l_2^2)\ddot{\theta_2} - m_2 l_1 l_2 \dot{\theta_2}^2 \sin(\theta_2) \quad (A23)$$

$$\frac{\partial L}{\partial \theta_1} = -(m_1+m_2) g l_1 \cos(\theta_1) - m_2 g l_2 \cos(\theta_1+\theta_2) \quad (A24)$$

$$\frac{d}{dt}\left(\frac{\partial l}{\partial \dot{\theta_1}}\right) - \frac{\partial L}{\partial \theta_1} = \tau_1 \quad (A25)$$

$$((m_1 + m_2)l_1^2 + 2m_2 l_1 l_2 \cos(\theta_2) + m_2 l_2^2)\ddot{\theta_1} - 2m_2 l_1 l_2 \dot{\theta_1}\dot{\theta_2}\sin(\theta_2) + (m_2 l_1 l_2 \cos(\theta_2) + m_2 l_2^2)\ddot{\theta_2} - m_2 l_1 l_2 \dot{\theta_2}^2 \sin(\theta_2) + (m_1+m_2) g l_1 \cos(\theta_1) + m_2 g l_2 \cos(\theta_1+\theta_2) = \tau_1 \quad (A26)$$

$$\frac{\partial L}{\partial \dot{\theta_2}} = (m_2 l_1 l_2 \cos(\theta_2) + m_2 l_2^2)\dot{\theta_1} + m_2 l_2^2 \dot{\theta_2} \quad (A27)$$

$$\frac{d}{dt}\left(\frac{\partial l}{\partial \dot{\theta_2}}\right) = (m_2 l_1 l_2 \cos(\theta_2) + m_2 l_2^2)\ddot{\theta_1} - m_2 l_1 l_2 \dot{\theta_1}\dot{\theta_2}\sin(\theta_2) + m_2 l_2^2 \ddot{\theta_2} \quad (A28)$$

$$\frac{\partial L}{\partial \theta_2} = -m_2 l_1 l_2 \sin(\theta_2)\dot{\theta_1}^2 - m_2 l_1 l_2 \sin(\theta_2)\dot{\theta_1}\dot{\theta_2} - m_2 g l_2 \cos(\theta_1+\theta_2) \quad (A29)$$

$$\frac{d}{dt}\left(\frac{\partial l}{\partial \dot{\theta_2}}\right) - \frac{\partial L}{\partial \theta_2} = \tau_2 \quad (A30)$$

$$(m_2 l_1 l_2 \cos(\theta_2) + m_2 l_2^2)\ddot{\theta_1} - m_2 l_1 l_2 \dot{\theta_1}\dot{\theta_2}\sin(\theta_2) + m_2 l_2^2 \ddot{\theta_2} + m_2 l_1 l_2 \sin(\theta_2)\dot{\theta_1}^2 + m_2 l_1 l_2 \sin(\theta_2)\dot{\theta_1}\dot{\theta_2} + m_2 g l_2 \cos(\theta_1+\theta_2) \quad (A31)$$

$$(m_2 l_1 l_2 \cos(\theta_2) + m_2 l_2^2)\ddot{\theta_1} + m_2 l_2^2 \ddot{\theta_2} + m_2 l_1 l_2 \sin(\theta_2)\dot{\theta_1}^2 + m_2 g l_2 \cos(\theta_1+\theta_2) = \tau_2 \quad (A32)$$